Negative differential resistance in parallel single-walled carbon nanotube contacts

Qihang Liu,[1] Guangfu Luo,[1] Rui Qin,[1] Hong Li,[1] Xin Yan,[1] Chengyong Xu,[1] Lin Lai,[1] Jing Zhou,[1] Shimin Hou,[2] Enge Wang,[1] Zhengxiang Gao,[1] and Jing Lu[1,*]

[1]*State Key Laboratory for Mesoscopic Physics and Department of Physics, Peking University, Beijing 100871, People's Republic of China*

[2]*Key Laboratory for the Physics and Chemistry of Nanodevices, Department of Electronics, Peking University, Beijing 100871, People's Republic of China*

(Received 6 November 2010; published 26 April 2011)

Based on first-principles calculations, we investigate the electron transport properties of parallel single-walled carbon nanotube contact. A significant negative differential resistance (NDR) behavior is found due to staggered electron gratings in energy space and standing waves in real space on the two tubes induced by bias. Such a NDR effect is robust against the contact length, the tube diameter, the shape of the end, and the difference in the two electrodes. Because no bridging molecule is used, the structure of this NDR device is simpler compared with ordinary molecular NDR devices. Our findings are expected to promote the discovery of more NDR devices composed of only two electrodes in parallel contact.

DOI: 10.1103/PhysRevB.83.155442 PACS number(s): 73.63.Rt, 72.10.Fk, 72.20.Ht

I. INTRODUCTION

Negative differential resistance (NDR) is widely utilized in a variety of traditionalelectronic devices such as oscillators, amplifiers, frequency mixers, logic cells, and memories. NDR in a nanoscale molecular device was discovered in thiol molecules on gold surfaces via scanning tunneling microscopy (STM) in 1999.[1,2] However, the poorly defined bonding between a molecule and metal electrodes causes irreproducibility of the metal-molecule junction,[3,4] which leads to divergence between experiment and theoretical studies.[5–8] Alternatively, nonmetal Si and single-walled carbon nanotubes (SWNTs) are used as electrodes in molecular electronic devices due to the well-defined bonding between Si/SWNT and organic molecules.[9–19] NDR at room temperature has been observed in organic molecules on Si(100) surfaces by ultrahigh vacuum STM,[9] and subsequent calculations based on density functional theory (DFT) coupled with nonequilibrium Green's function (NEGF) method corroborate NDR in Si-organic molecule junctions.[11] During the shrinking of a carbon nanotube in vacuum, NDR is observed when the diameter of the carbon nanotube is reduced to near zero, the limit of a carbon atomic wire.[13] Subsequent first-principles scattering-state calculations confirm that the carbon chains covalently connecting metallic SWNT electrodes can induce NDR.[14] By using DFT+NEGF calculations, NDR is also predicted in other SWNT-molecule junctions by noncovalently coupling an anthracene molecule[15] and covalently coupling a pyrrolopyrrole molecule through amide, ester, and imide linkages.[16,17]

So far the NDR phenomenon in molecular electronics is closely dependent on the junction between the molecule and electrodes. One fundamental and intriguing question arises: Is it possible to generate NDR without any bridging molecule or wire between the two nanoscale electrodes? In this article, by first-principles transport calculations, we show that NDR behavior can exist in two metallic SWNTs in parallel contact, without any molecule or wire bridging two electrodes. Such a NDR effect is rather robust against the contact length, the tube diameter, the shape of the end, and the difference in the two electrodes. Besides, the current drop of NDR region in this simplest molecular device can exceed 20 μA, which is one to two orders of magnitude greater than those in most SWNT-based NDR devices.[14–16]

II. METHOD

The transport properties are calculated by the ATOMISTIX TOOLKIT 2008.10 code,[20,21] which is based on the combination of DFT as implemented in the SIESTA code[22] with NEGF method. The local-density approximation (LDA)[23] to the exchange-correlation functional and norm-conserving pseudopotentials are used.[24] A single-ζ plus polarization orbital basis set is employed and the convergence criterion for the total energy is 10^{-5} Ry to achieve a balance between calculation efficiency and accuracy. The lateral size of the supercell is 25×25 Å so that the intertube interaction is negligible. The mesh cutoff is chosen as 150 Ry, and a Monkhorst-Pack k mesh of $1\times1\times500$ is used. The electron temperature is set to 300 K. The system is divided into three parts; left electrode, scattering region (SR), and right electrode. The transmission spectrum can be calculated from the Green's function approach:

$$T(E) = \mathrm{Tr}[t^{\dagger}t] = \mathrm{Tr}[\Gamma_L G^r \Gamma_R G^{r\dagger}]. \quad (1)$$

Here t is the transmission matrix, G^r and $\Gamma_{L_{(R)}}$ represent the retarded Green's function in the SR and the coupling matrix between the left (right) electrode and the SR:

$$G^r = (ES - H - \Sigma_L - \Sigma_R)^{-1}, \quad (2)$$

$$\Gamma_{L(R)} = i(\Sigma_{L(R)} - \Sigma^{\dagger}_{L(R)}), \quad (3)$$

where $\Sigma_{L_{(R)}}$ is the corresponding self-energy term. For the system at equilibrium, the conductance G is evaluated by the following

$$G = G_0 T(E_f), \quad (4)$$

where $G_0 = 2e^2/h$ is the conductance quantum. The current is calculated using the Landauer-Büttiker formula by integrating the transmission spectrum between the two chemical potentials of the electrodes:[25]

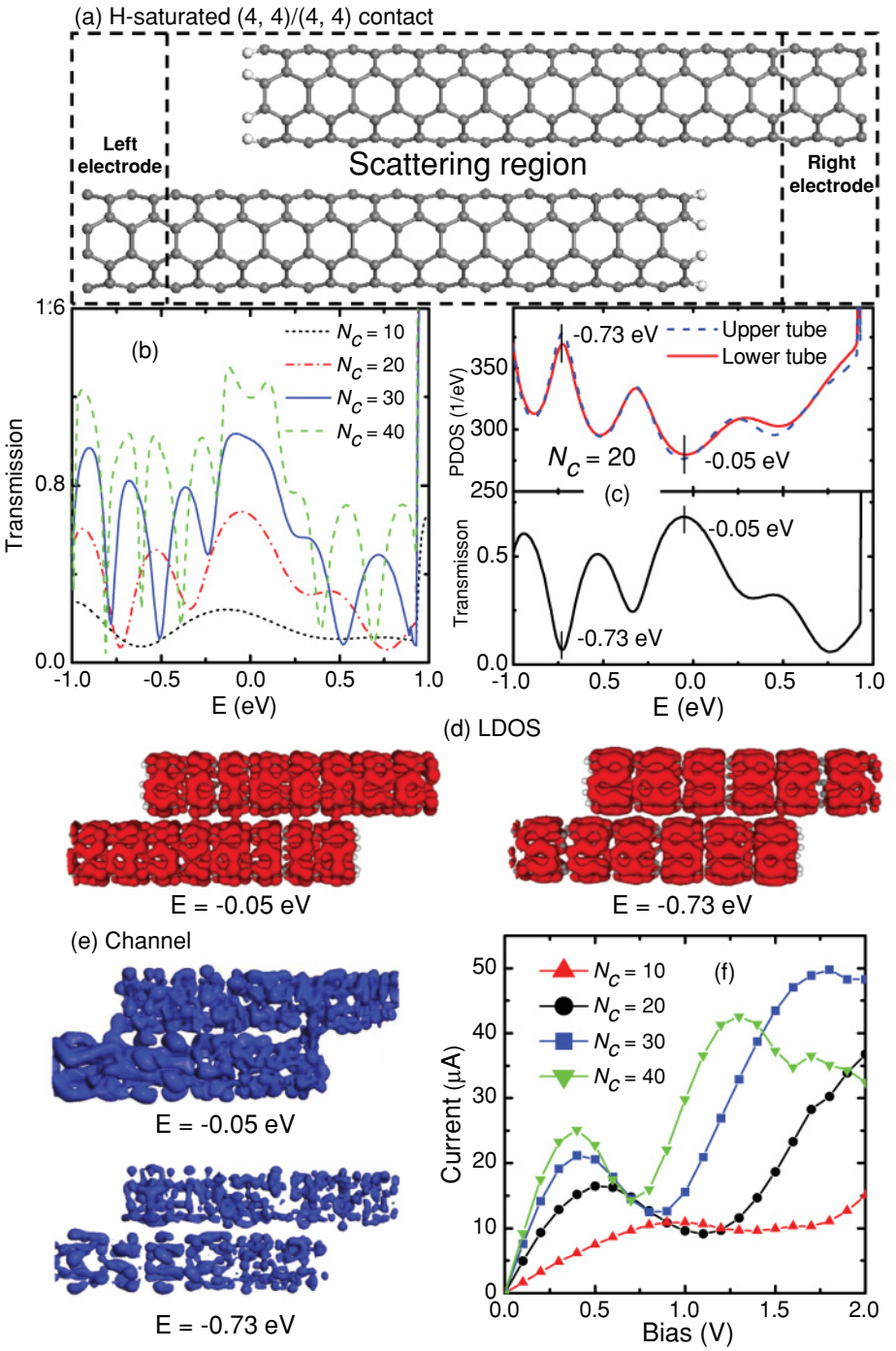

FIG. 1. (Color online) H-saturated (4,4)/(4,4) parallel contact. (a) Two-probe model. (b) Zero-bias transmission spectra. (c) PDOSs of the upper and lower tube of the contact area and zero-bias transmission with a contact length of $N_c = 20$. (d) LDOSs at the extended and quasibound states with $N_c = 20$. The isovalue is 0.0015 a.u. (e) Conductive transmission eigenchannels at the extended and quasibound states with $N_c = 20$. The isovalue is 0.007 a.u. (f) *I-V* characteristics. Gray and white balls represent C and H atoms, respectively. The Fermi level is set to zero.

$$I(V) = \frac{2e}{h}\int_{-\infty}^{+\infty}\{T(E,V)[f_L(E-\mu_L) - f_R(E-\mu_R)]\}dE, \quad (5)$$

where $f_{L_{(R)}}$ is the Fermi-Dirac distribution function for the left (right) electrode, and $\mu_{L(R)} = E_f \pm \frac{V}{2}$ is the electrochemical potential of the left (right) electrode.

III. RESULTS AND DISCUSSION

A. Zero-bias transmission spectra and quasibound states

We start with the case that consists of two H-terminated (4,4) armchair SWNTs in parallel contact [labeled by (4,4)/(4,4) contact] [see Fig. 1(a)]. The ends are saturated by H atoms to eliminate the dangling bonds. The distance between

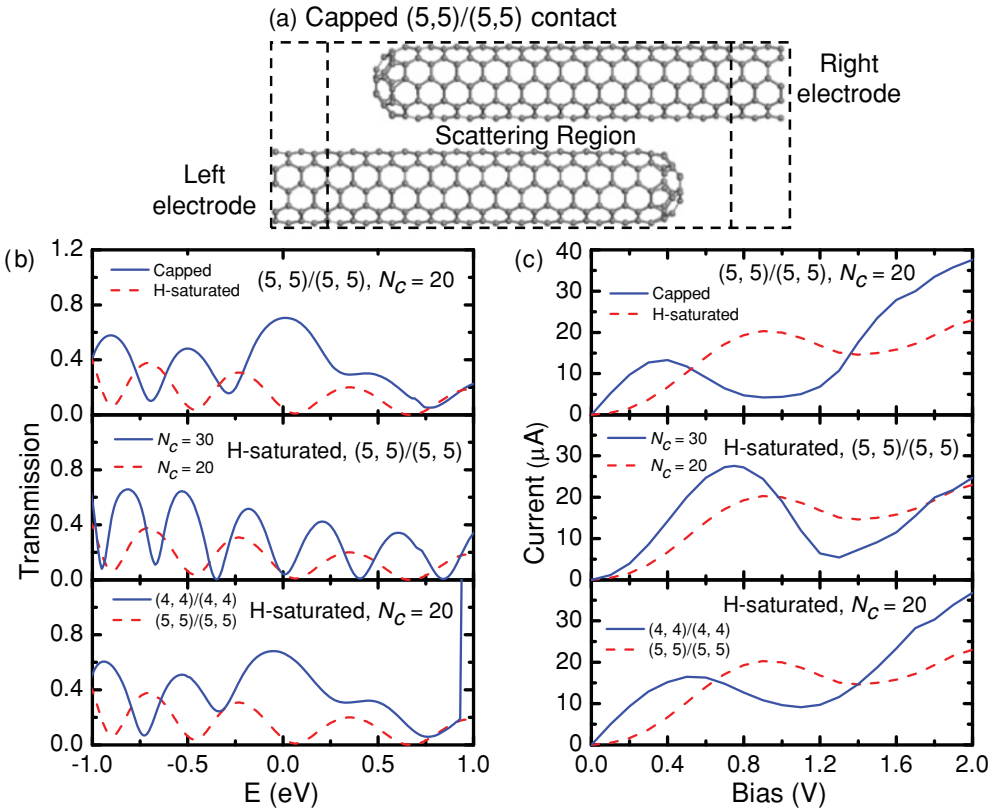

FIG. 2. (Color online) (a) Model of the capped (5,5)/(5,5) parallel contact, which is optimized until the force acting on each atom is <0.1 eV/Å. (b) Zero-bias transmission spectra and (c) *I-V* characteristics of the parallel contacts with different shapes of the end, contact lengths, and tube diameters. The Fermi level is set to zero.

the two SWNTs is fixed to 3.0 Å according to the equilibrium spacing of a bundle of SWNTs.[26] The transmission is not sensitive to small changes in the intertube distance around this value. First of all, we investigate the zero-bias transmission spectrum under different contact lengths (L_c, the overlapping length of the two tubes) measured by overlapping C atom layers (N_c) and show the results in Fig. 1(b). The maximum zero-bias transmission coefficient increases with L_c. When $L_c = 4.92$ nm or $N_c = 40$, the zero-bias conductance at the Fermi level (E_f) reaches 1.20 G_0 ($G_0 = 2e^2/h$). The maximum zero-bias conductance will approach that of a perfect SWNT ($2G_0$) from a simple linear extrapolation when L_c reaches 8.2 nm, compared with a value of ~10 nm obtained in a previous calculation.[27]

Oscillation is observed in the transmission spectra, and a similar phenomenon has been reported in the previous calculation.[27] The oscillation intensity increases with L_c, and the number of the transmission peaks is nearly proportional to the contact length. We plot the zero-bias projected density of states (PDOS) of the overlapping parts ($N_c = 20$) of the two tubes, respectively, in Fig. 1(c), and they nearly coincide owing to the symmetrical arrangement of the lower and upper tubes. Interestingly, the maxima and minima in the PDOS have a one-to-one correspondence with the minima and maxima in the transmission spectra. This clear correspondence suggests that relatively quasibound states are formed on the two tubes separately at the maxima of the PDOS, which scatter the incoming wave with identical energy (the scattering of the quasibound state to the incoming wave with identical energy is often referred to as resonant backscattering[27–29]) and result in the dips in the transmission spectrum. On the other hand, relatively extended states are formed on the two tubes separately at the minima of the PDOS, which allow the incoming wave to pass through and result in the peaks in the transmission spectrum.[27] This picture is further confirmed from the spatially resolved localized density of states (LDOS) of the contact area at $E = -0.05$ and -0.73 eV, which correspond to the transmission peak and valley, respectively, and are shown in Fig. 1(d). Both LDOSs are characterized by a standing-wave pattern due to a quantum interference of the incoming waves and the reflected ones by the finite end.[30] But the state at $E = -0.05$ eV appears more extendable than that at $E = -0.73$ eV because the values of the nodes of the latter state are much smaller and can divide the state into several discrete regions in real space. Therefore, electron grating is formed in the energy space of each tube. Besides, we notice that the antinodes of the two tubes face each other in the extended state while the nodes of the upper tube face the antinodes of the lower tube in the quasibound state. As a result, there is larger overlap between the extended states on the two tubes compared with the quasibound state. This factor further enhances the transmission coefficient of the extended state. There are two eigenchannels contributing to the total transmission: One is conductive and the other is almost totally closed. The conductive transmission eigenchannels of the extended state at $E = -0.05$ eV and quasibound state at

$E = -0.73$ eV are displayed in Fig. 1(e), and it is apparent that the electron has much larger probability to reach the upper tube in the extended state than in the quasibound state.

B. *I-V* characteristics

The *I-V* characteristics of the H-saturated (4,4)/(4,4) contact are shown in Fig. 1(f). Remarkable NDR effects appear at four different contact lengths, and there are even two current dips at $N_c = 30$ and $N_c = 40$ in the bias range of $V = 0$–2 V. In general, the NDR effects have lower onset biases, larger current drops, and smaller bias differences between the adjacent NDR peaks when N_c increases. The onset bias decreases from $V_{\text{onset}} = 1.0$ V for $N_c = 10$ to 0.5 V at $N_c = 20$ and 0.4 V at $N_c = 30$ and $N_c = 40$. The current drops of the NDR are $I_{\text{drop}} = 1.3$, 7.4, and 8.7 μA, and 10.8 μA at $N_c = 10$, 20, 30, and 40, respectively, and the latter three values are one to two orders of magnitude greater than those in most SWNT-based NDR devices.[14–16] The peak-to-valley ratios (PVRs) are 1.13, 1.81, 1.70, and 1.76 at $N_c = 10$, 20, 30, and 40, respectively. Generally speaking, NDR effects are enhanced with increasing N_c.

The model of the capped (5,5) SWNT in parallel contact is shown in Fig. 2(a). The zero-bias transmission spectra and *I-V* characteristics of the (5,5)/(5,5) contact with different end shapes and contact lengths are shown in Figs. 2(b) and 2(c), respectively. Oscillation character of the zero-bias transmission spectra and NDR effects remains. The maximum zero-bias transmission coefficient is doubled after the end is capped at $N_c = 20$, but the oscillation frequency of the transmission spectra remains unchanged except for a phase shift of half period. V_{onset} decreases from 0.9 to 0.4 V, I_{drop} increases from 5.7 to 9.1 μA, and PVR increases from 1.39 to 2.78 upon capping the end; therefore, NDR effect is enhanced upon capping the end. The maximum zero-bias transmission coefficient and the NDR effects remain enhanced in terms of a decrease in V_{onset} from 0.9 to 0.7 V and increases in I_{drop} from 5.7 to 21.0 μA and in PVR from 1.39 to 5.08 when the contact length increases from $N_c = 20$ to 30 in the H-saturated (5,5) contact. Given the same N_c, the oscillation frequency of the transmission spectra remains unchanged between the H-saturated (4,4)/(4,4) and (5,5)/(5,5) contacts except for a phase shift of half period. The NDR effects are generally weaken from the (4,4) to (5,5) tube at $N_c = 20$ in terms of decreases in I_{drop} from 7.4 to 5.7 μA and in PVR from 1.81 to 1.39, but are enhanced at $N_c = 30$ in terms of increases in I_{drop} from 8.7 to 21.9 μA and in PVR from 1.70 to 5.08.

C. Origin of the NDR effect

Next we take the H-saturated (4,4)/(4,4) parallel contact with $N_c = 20$ as an example to explore the origin of the NDR effect in the parallel SWNT contact. We plot the bias-dependent transmission spectra, PDOSs of the overlapping parts of the two tubes, LDOSs, and the transmission channels of the contact area in Fig. 3. At zero bias, the coincidence

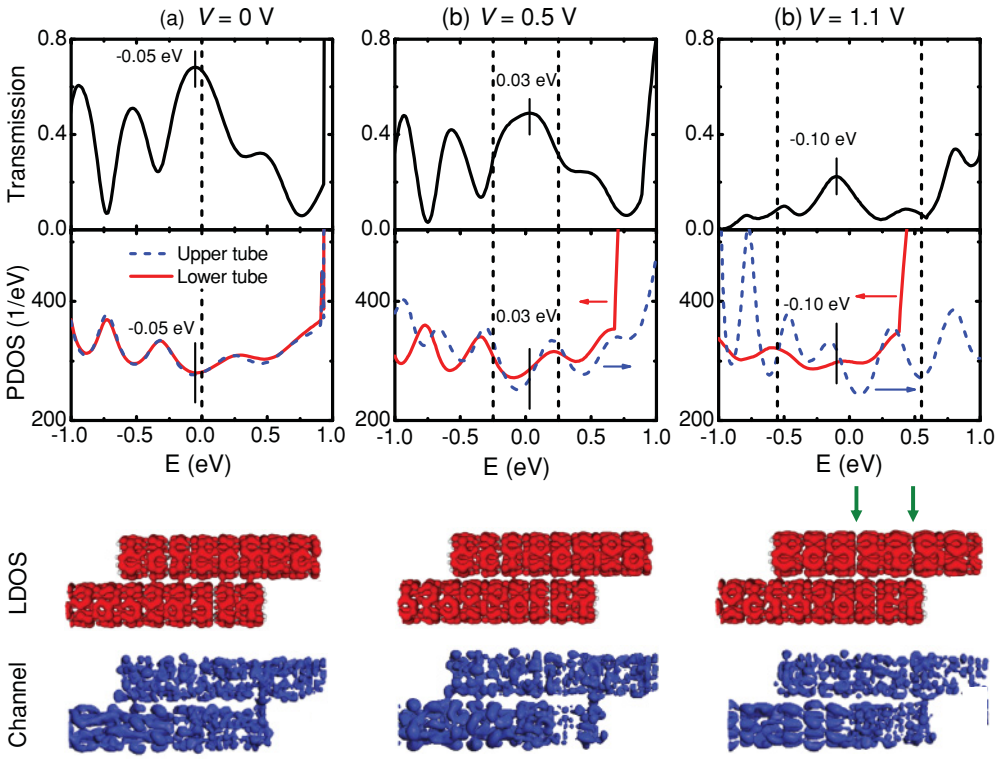

FIG. 3. (Color online) Transmission spectra, PDOSs of the overlapping parts of the two tubes, LDOSs (isovalue is 0.0015 a.u.), and conductive transmission eigenstates (isovalue is 0.015 a.u.) at the prominent transmission peaks around E_f of the H-saturated (4,4)/(4,4) parallel contact with $N_c = 20$ under different biases: (a) 0 V, (b) 0.5 V, and (c) 1.1 V. The Fermi level is set to zero. The black dashed lines in the transmission spectra represent the bias windows, and the red and blue arrows indicate the shift directions of the electron states of the lower and upper tubes, respectively. The green arrows indicate the positions of the breaking points of the LDOS induced by bias.

of the PDOSs of the lower and upper tubes indicates that the extended states (quasibound states) belonging to the two tubes always appear in the same energy, just like two eclipsed electron gratings in energy space. In this example, there is a transmission coefficient maximum at $E=-0.05$ eV, and the differential conductance has a maximum at zero bias [see Fig. 1(f)]. After bias is applied, the lower tube feels a positive electrostatic potential while the upper tube feels a negative one, and the electronic states of the lower tube shift towards the lower energy direction and those of the upper tube shifts towards the higher energy direction. At a small bias of $V=0.5$ V, the energy shifts of the electronic states of both tubes are small, and this small mismatch of the two electron gratings causes a slight reduction of the transmission coefficients within the bias window. The current actually peaks at this bias. The PDOSs of both tubes corresponding to the transmission peak (at $E=0.03$ eV) within the bias window are in the mountainside, and the electronic states at $E=0.03$ eV of the two tubes are identified as extended states from their continuous LDOS distribution. However, the nodes of the standing wave of the LDOS of the lower tube face the antinodes of that of the upper tube, and the staggered standing waves of the LDOSs on the two tubes in real space appears to be another factor responsible for the reduction in the transmission coefficient.

When V increases to 1.1 V, the electronic state of the upper tube of the transmission maximum (at $E=-0.10$ eV) within the bias window is localized from its large PDOS peak and discrete LDOS while the electronic state of the lower tube remains extended. Such a staggered electron localization arises from staggered (partially or completely) arrangement of the electron gratings on the two tubes. Consequently, electrons have smaller probability to reach the upper tube at $E=-0.10$ eV, as reflected from the transmission channel and greatly depressed transmission peak. At $E=0.08$ eV, the PDOSs of the two tubes correspond to valleys, and the electrons of both tubes are in extended state. In other words, the two electron gratings are partially staggered at this bias. The staggered arrangement of the standing waves of the LDOSs on the two tubes appears to be dominantly responsible for the reduction in the transmission coefficient at this energy (see Fig. S1).[31] In the whole bias window (−0.55 to 0.55 V), the greatly depressed transmission coefficients are attributed to either the staggered electron localization or the staggered standing waves of the LDOSs on the two tubes. Consequently, I is reduced at $V=1.1$ V, compared with at $V=0.5$ V, and the first NDR phenomenon appears. The bias dependences of the transmission spectra and PDOS of the capped (5,5)/(5,5) with $N_c=20$ are provided in Fig. S2,[31] and the NDR effects therein can be understood chiefly in terms of two staggered electron gratings in energy space.[31]

When the bias further increases, the two electron gratings (and LDOSs) are eclipsed again and I continually increases. At a large enough bias, the two electron gratings are staggered once more, and the second NDR phenomenon will take place. As an example, the transmission spectra and PDOSs of the overlapping parts of the two tubes of the H-saturated (4,4)/(4,4) parallel contact with $N_c=40$ under different biases

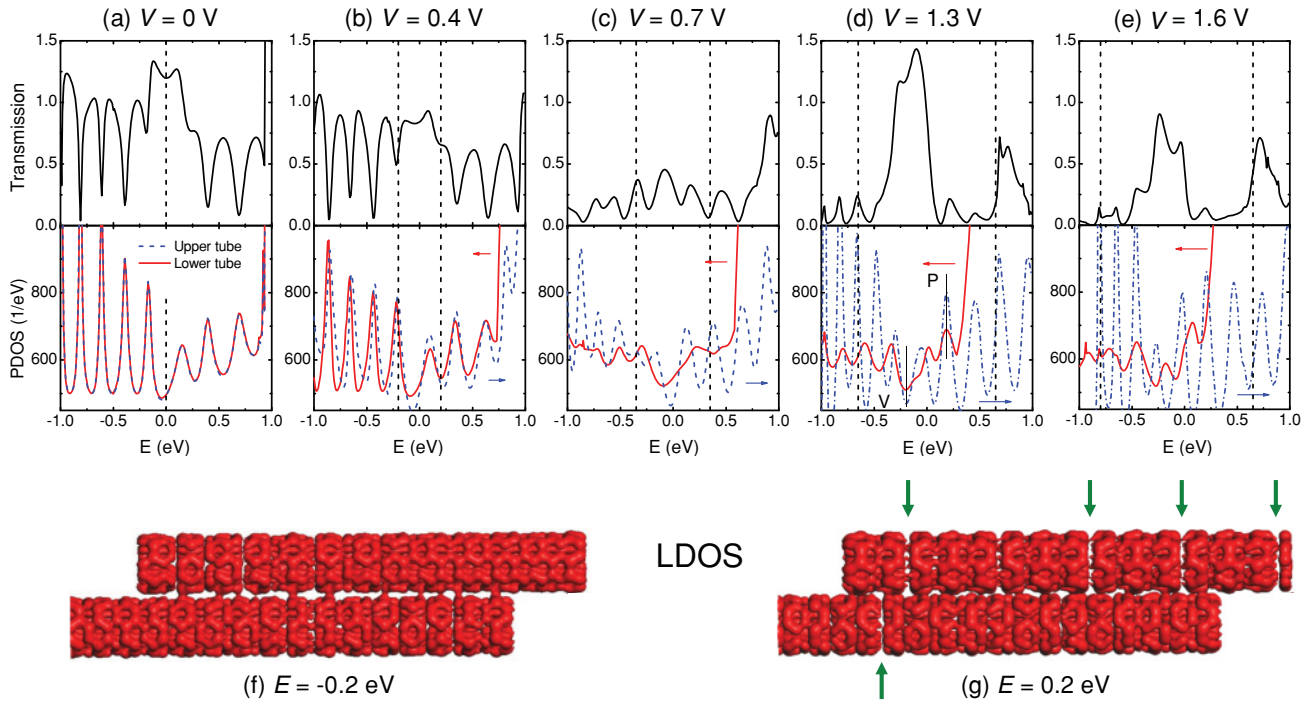

FIG. 4. (Color online) (a)–(e) Transmission spectra and PDOSs of the overlapping parts of the two tubes of the H-saturated (4,4)/(4,4) parallel contact with $N_c=40$ under different biases of (a) 0 V, (b) 0.4 V, (c) 0.7 V, (d) 1.3 V, and (e) 1.6 V. LDOS at (f) $E=-0.2$ eV (PDOS valley position) and (g) at $E=0.2$ eV (PDOS peak position) at $V=1.3$ V. The Fermi level is set to zero. The black dashed lines in the transmission spectra represent the bias windows, and the red and blue arrows indicate the shift directions of the electron states of the lower and upper tubes, respectively. The green arrows indicate the positions of the breaking points of the LDOSs.

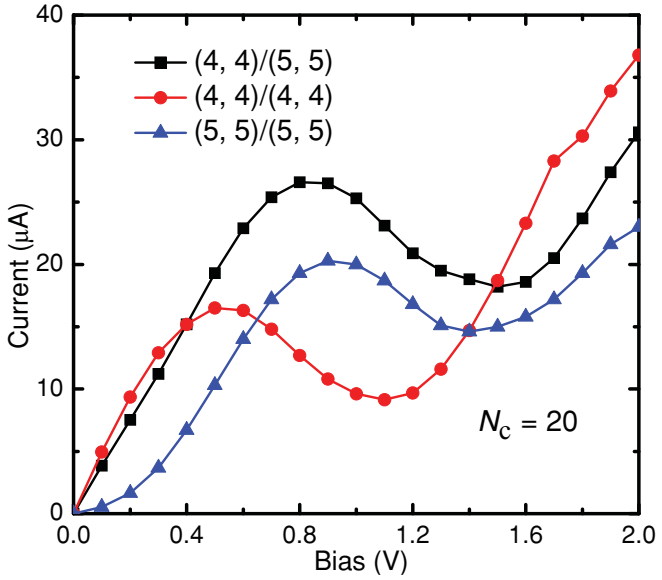

FIG. 5. (Color online) *I-V* characteristic of the H-saturated (4,4)/(5,5) heterogeneous parallel contact with $N_c = 20$, and those of the H-saturated (4,4)/(4,4) and (5,5)/(5,5) homogeneous parallel contacts are also plotted for comparison.

and LDOSs are shown in Fig. 4. At the bias range of 0– 0.4 V, the relative movement of the two electron gratings is small, the transmission spectra do not change significantly, and the current increases with the bias [see Fig. 1(f)]. At $V = 0.7$ V, the transmission coefficients within the bias window are greatly depressed due to the staggered arrangement of the two electron gratings, and the first NDR effect appears. When the bias increases to 1.3 V, the two electron gratings have eclipsed configuration in the energy range of -0.3 to 0.2 eV. The LDOSs of the two tubes at $E = -0.2$ eV (V point) are highly continuous on the region close to the electrodes despite a staggered arrangement and ensure a large transmission peak and the current upturn. The LDOSs of the upper and lower tubes at $E = 0.2$ eV (P point) are localized (the localization of the upper tube is especially apparent), causing a small transmission coefficient. As for $V = 1.6$ V, the two electron gratings are staggered (nearly completely) again, leading to the depression of the prominent transmission peak and the second NDR. In addition, we note that the energy separation between two adjacent extended and quasibound states decreases with the increasing N_c, and this is responsible for the increasing transmission peak number with the increasing N_c. Given a larger contact length, a smaller bias is required to give rise to staggered electron gratings on the two tubes. Therefore, increasing the contact length tends to reduce the onset voltage of NDR and the voltage difference between the adjacent NDR peaks.

D. DISCUSSION

It is interesting to examine the validity of NDR in a heterogeneous parallel SWNT contact. We construct a heterogeneous parallel contact by using the H-saturated (4,4) and (5,5) SWNTs as the two electrodes, respectively. The *I-V* characteristics of the H-saturated (4,4)/(5,5) parallel contact with $N_c = 20$ are shown in Fig. 5. Obvious NDR effect is observed at $V = 0.8$–1.5 V, with an onset bias between those of the (4,4)/(4,4) and (5,5)/(5,5) contacts. The current drop of the (4,4)/(5,5) heterogeneous parallel contact is $I_{\text{drop}} = 8.4$ μA, larger than those of the two homogeneous parallel contacts with the same contact length [$I_{\text{drop}} = 7.4$ and 5.7 μA for the (4,4)/(4,4) and (5,5)/(5,5) contacts, respectively]. The transmission spectra and PDOSs under various bias voltages of the H-saturated (4,4)/(5,5) parallel contact with $N_c = 20$ are shown in Fig. S3.[31] The NDR exists not only in the H-saturated SWNT contact but also exists in the H-free homogeneous and heterogeneous parallel SWNT contacts with dangling bonds at the finite ends of the SWNTs, as shown in Fig. 6. Therefore, NDR in the parallel SWNT contact is robust against the existence of dangling bonds. In addition, we have also performed transport calculations with one tube rotated around the tube axis to examine the effect of relative rotation between the two tubes. It is found that the transmission spectra change little for different rotation angles, except for the case that the system has a symmetry mirror plane which contains the two tube axes. As a result of the common symmetry mirror plane of the two tubes, the conductance channels due to both of the

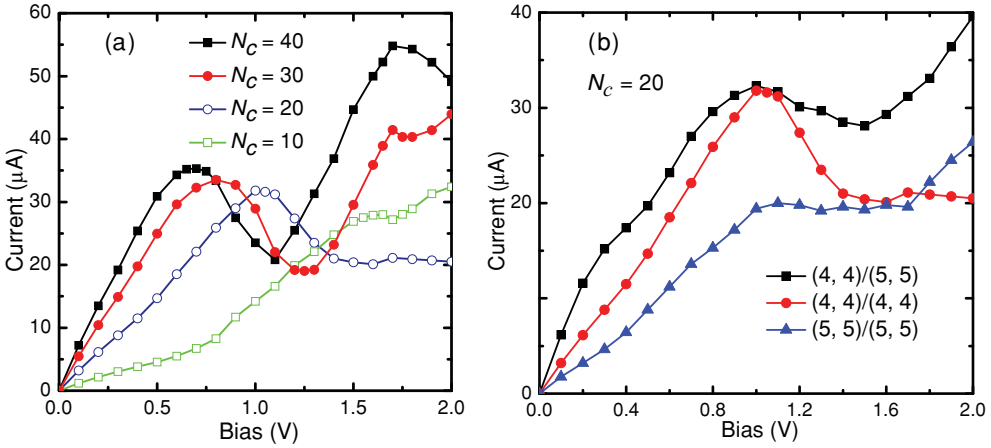

FIG. 6. (Color online) *I-V* characteristics of the H-free open-ended parallel contacts. (a) (4,4)/(4,4) homogeneous contacts and (b) (4,4)/(5,5) heterogeneous contact with $N_c = 20$. The *I-V* curves of (4,4)/(4,4) and (5,5)/(5,5) homogeneous contacts are also plotted for comparison.

π band and the π^* band become more open, and the symmetry match leads to larger transmission probability from one SWNT to the other. However, the positions of maxima and minima in the transmission spectra, e.g., the extended and quasibound states are invariable with the rotation angles, and thus NDR also stably exists under relative rotation of the two tubes.

IV. CONCLUSION

In conclusion, by using DFT+NEGF calculations, we report a nanoscale NDR device which consists of only two metallic SWNTs in parallel contact, without any molecule or wire bridging the electrodes. This NDR device has two exceptional advantages. First, this NDR device is simplified compared to the ordinary molecular NDR devices. Besides, the NDR effect is rather robust against the contact length, the tube diameter, the shape of the end, and the difference in the two electrodes. Electron grating and standing waves are formed in energy space and real space, respectively, on each tube, and bias causes a movement of the two electron gratings and standing waves on the two tubes. The physical origin of NDR in this device is attributed to formation of staggered electron gratings in energy space and standing waves of the LDOSs in real space on the two tubes induced by bias, which greatly prevent electrons from transmitting. One can take advantage of the staggered electron gratings in energy space or standing waves of the LDOSs in real space to design other NDR devices generated directly by two electrodes with parallel contact, like telescopically aligned double-walled nanotube (DWNT) contact or parallel graphene nanoribbon contact. Up to now, we have already confirmed that robust NDR effect also exists in telescoping DWNT contacts, with a mechanism similar to that discussed in this paper.[32]

ACKNOWLEDGMENTS

This work was supported by the NSFC (Grants No. 10774003, No. 10474123, No. 10434010, No. 90606023, and No. 20731160012), National 973 Projects (No. 2002CB613505 and No. 2007CB936200, MOST of China), Fundamental Research Funds for the Central Universities, National Foundation for Fostering Talents of Basic Science (No. J0630311), and Program for New Century Excellent Talents in University of MOE of China. We thank X. F. Guo for helpful discussion.

*Author to whom correspondence should be addressed: jinglu@pku.edu.cn

[1] J. Chen, M. A. Reed, A. M. Rawlett, and J. M. Tour, Science **286**, 1550 (1999).
[2] Y. Xue, S. Datta, S. Hong, R. Reifenberger, J. I. Henderson, and C. P. Kubiak, Phys. Rev. B **59**, R7852 (1999).
[3] H. Basch, R. Cohen, and M. A. Ratner, Nano Lett. **5**, 1668 (2005).
[4] L. Venkataraman, J. E. Klare, I. W. Tam, C. Nuckolls, M. S. Hybertsen, and M. L. Steigerwald, Nano Lett. **6**, 458 (2006).
[5] S.-H. Ke, H. U. Baranger, and W. T. Yang, J. Chem. Phys. **122**, 074704 (2005).
[6] P. Delaney and J. C. Greer, Phys. Rev. Lett. **93**, 036805 (2004).
[7] M. Di Ventra, S. G. Kim, S. T. Pantelides, and N. D. Lang, Phys. Rev. Lett. **86**, 288 (2001).
[8] M. Di Ventra, S. T. Pantelides, and N. D. Lang, Phys. Rev. Lett. **84**, 979 (2000).
[9] N. P. Guisinger, M. E. Greene, R. Basu, A. S. Baluch, and M. C. Hersam, Nano Lett. **4**, 55 (2004).
[10] T. Rakshit, G. C. Liang, A. W. Ghosh, and S. Datta, Nano Lett. **4**, 1803 (2004).
[11] W. C. Lu, V. Meunier, and J. Bernholc, Phys. Rev. Lett. **95**, 206805 (2005).
[12] S.-H. Ke, H. U. Baranger, and W. T. Yang, Phys. Rev. Lett. **99**, 146802 (2007).
[13] T. D. Yuzvinsky, W. Mickelson, S. Aloni, G. E. Begtrup, A. Kis, and A. Zettl, Nano Lett. **6**, 2718 (2006).
[14] K. H. Khoo, J. B. Neaton, Y. W. Son, M. L. Cohen, and S. G. Louie, Nano Lett. **8**, 2900 (2008).
[15] Y. Xu, G. Zhang, and B. W. Li, J. Phys. Chem. B **112**, 16891 (2008).
[16] W. Y. Kim, S. K. Kwon, and K. S. Kim, Phys. Rev. B **76**, 033415 (2007).
[17] W. Y. Kim, Y. C. Choi, and K. S. Kim, J. Mater. Chem. **18**, 4510 (2008).
[18] G. Buchs, P. Ruffieux, P. Groning, and O. Groning, Appl. Phys. Lett. **93**, 073115 (2008).
[19] S. U. Lee, R. V. Belosludov, H. Mizuseki, and Y. Kawazoe, Small **5**, 1769 (2009).
[20] J. Taylor, H. Guo, and J. Wang, Phys. Rev. B **63**, 245407 (2001).
[21] M. Brandbyge, J. L. Mozos, P. Ordejon, J. Taylor, and K. Stokbro, Phys. Rev. B **65**, 165401 (2002).
[22] P. Ordejon, E. Artacho, and J. M. Soler, Phys. Rev. B **53**, 10441 (1996).
[23] J. P. Perdew and A. Zunger, Phys. Rev. B **23**, 5048 (1981).
[24] N. Troullier and J. L. Martins, Phys. Rev. B **43**, 1993 (1991).
[25] M. Buttiker, Y. Imry, R. Landauer, and S. Pinhas, Phys. Rev. B **31**, 6207 (1985).
[26] W. S. Liu, G. F. Luo, H. Li, L. Wang, J. Lu, J. Zhou, R. Qin, Z. X. Gao, and L. Lai, J. Nanosci. Nanotechnol. **9**, 5170 (2009).
[27] C. Buia, A. Buldum, and J. P. Lu, Phys. Rev. B **67**, 113409 (2003).
[28] H. J. Choi, J. Ihm, S. G. Louie, and M. L. Cohen, Phys. Rev. Lett. **84**, 2917 (2000).
[29] B. Biel, X. Blase, F. Triozon, and S. Roche, Phys. Rev. Lett. **102**, 096803 (2009).
[30] A. Rubio, D. Sanchez-Portal, E. Artacho, P. Ordejon, and J. M. Soler, Phys. Rev. Lett. **82**, 3520 (1999).
[31] See supplemental material at [http://link.aps.org/supplemental/10.1103/PhysRevB.83.155442] for the further analyses of the transport properties of different parallel SWNT contacts.
[32] Q. H. Liu, L. L. Yu, H. Li, R. Qin, J. Zhou, J. X. Zheng, Z. X. Gao, and J. Lu, J. Phys. Chem. C **115**, 6933 (2011).